Nonlinear density waves on graphene electron fluids

Pedro Cosme * and Hugo Terças
GoLP/Instituto de Plasmas e Fusão Nuclear, Instituto Superior Técnico, Lisboa 1049-001, Portugal

(Received 7 March 2023; accepted 16 May 2023; published 24 May 2023)

The hydrodynamic behavior of charged carriers leads to nonlinear phenomena such as solitary waves and shocks, among others. As an application, such waves might be exploited on plasmonic devices either for modulation or signal propagation along graphene waveguides. We study the nature of nonlinear perturbations following an approach similar to Sagdeev potential analysis and also by performing the reductive perturbation method on the hydrodynamic description of graphene electrons, taking into consideration the effect of Bohm quantum potential and odd viscosity. Thus, deriving a dissipative Kadomtsev-Petviashvili-Burgers (KPB) equation for the bidimensional flow as well as its unidimensional limit in the form of Korteweg–de Vries–Burgers (KdVB). The stability analysis of these equations unveils the existence of unstable modes that can be excited and launched through graphene plasmonic devices.

DOI: 10.1103/PhysRevB.107.195432

I. INTRODUCTION

The advent of graphene, and other two-dimensional materials, opened the way for remarkable and exciting physics and phenomena, particularly in the domains of charge transport and plasmonics where high mobility of electrons is required. Such areas are crucial to the development of next-generation devices that are compatible with integrated circuit technology [1], such as transistors [2], quantum dots [3], radiation detectors, and emitters or waveguides [4]. Indeed, the absence of gap in monolayer graphene, being problematic for digital devices, placed the focus of research on continuous wave applications, especially in the highly sought after THz range [5]. Much of the research on the THz problem in graphene devices take place within the hydrodynamic framework [5–8], a feature that has been motivated by the recent theoretical and experimental works supporting the hydrodynamic regime of electrons in graphene [9–16]. Recent works in graphene hydrodynamics involve viscometry [17,18], electron-phonon coupling [19,20], and nonlocal resistivity [21–23]. Consequently, the investigation of hydrodynamic plasmonic instabilities has received a new breath within the different communities, namely through mechanisms such as Coulomb drag [24,25], and Dyakonov-Shur and Ryzhii-Satou-Shur instabilities [26–29], the plasmonic boom instability [30] and surface-plasmon polaritons [31,32].

A prominent advantage of the hydrodynamic formulation of graphene electrons in respect to the quantum kinetic formulations is the study of nonlinear phenomena: the hydrodynamic equation is more suitable for analytical and numerical methods [33], despite ignoring some microscopic aspects of the momentum distributions in out-of-equilibrium situations. Though the nonlinear effects in optical setups—resorting to surface plasmon polaritons—have been reported [34–36], the study of nonlinear dynamics in graphene plasmonic systems is still elusive.

In this article, we explore the dynamics of nonlinear electron waves in graphene field-effect transistors (gFETs) within the framework of the hydrodynamic transport, achievable provided the following scale separation between the electron-electron free path (ℓ_{e-e}), the inelastic free path ($\ell_{e-\mathrm{imp}}$), and the system size (L) [9,10]

$$\ell_{e-e} \ll L \ll \ell_{e-\mathrm{imp}}, \tag{1}$$

a condition that has been reported in several experimental papers [12–15]. Despite the apparent simplicity of treating the electron transport in graphene via hydrodynamic equations, there are three major points which set this models apart from regular hydrodynamics. The first one is the fact that the effective mass is *compressible and relativistic*, i.e., depends on the number density n and on the flow speed $v = |\mathbf{v}|$ as [37]

$$\mathcal{M} = \frac{m^\star}{1 - v^2/v_F^2}, \tag{2}$$

where $m^\star = \hbar\sqrt{\pi n}/v_F$ is the Drude mass [10,29,38]. Secondly, the existence of a nondiffusive, odd viscosity term, arising in two-dimensional systems with broken time-reversal symmetry [39], arising either from the presence of magnetic fields [40,41] or from anisotropy of the Fermi sphere [42]. Finally, it has recently introduced corrections in the form of a quantum (Bohm) potential [43,44], which can be obtained from a more complete quantum kinetic description [37]. All of these factors contribute to a peculiar competition between dispersion and nonlinearity in the graphene hydrodynamics, which has profound implications in the physics of the nonlinear, as we explain below.

In order to examine the several possibilities that lead to nonlinear waves, this work is organized in the following manner: in Sec. II, the base hydrodynamical model is presented; then, in Sec. III, we derive the Hamiltonian description of

*pedro.cosme.e.silva@tecnico.ulisboa.pt

finite amplitude one-dimensional waves in the absence of viscosity. In Sec. IV, we proceed to a perturbative method that allows us to deal with viscous terms, and finally, concluding remarks are presented in Sec. V.

II. GRAPHENE HYDRODYNAMIC MODEL

We consider monolayer graphene in the field-effect transistor (FET) configuration, in which the gate—located at a distance d_0 away from the graphene sheet—effectively screens the Coulomb interaction between carriers [28]. In the fully degenerate limit, where the Fermi temperature is much higher than room temperature, the flow of electrons in gated graphene can be described by the following hydrodynamic model [29,37], comprising the continuity equation

$$\frac{\partial n}{\partial t} + \nabla\cdot(n\mathbf{v}) = 0, \tag{3}$$

and the momentum conservation equation

$$\frac{\partial}{\partial t}(nm^\star\mathbf{v}) + \nabla\cdot(nm^\star\mathbf{v}\otimes\mathbf{v}) + \nabla\cdot\mathbf{\Pi} + en\nabla\phi + \frac{\mathcal{B}m_0^\star}{\sqrt{n_0}}\nabla\cdot(\nabla\otimes\nabla\sqrt{n}) = 0. \tag{4}$$

Here, n and $\mathbf{v} = (u, v)$ are the density and the velocity fields, ϕ is the electrostatic potential, $\mathbf{\Pi}$ is the stress tensor. The last term in Eq. (4) is the quantum (Bohm) potential recently derived in Ref. [37], with magnitude governed by the quantum mechanical coefficient $\mathcal{B} = n_0\hbar^2/(32m_0^{\star 2})$, given in terms of the equilibrium density n_0 and equilibrium mass $m_0^\star$. The stress tensor comprises both the Fermi quantum pressure $p = \hbar v_F\sqrt{\pi n^3}/3$ and the shear and odd viscosities η_s and η_o such that [40]

$$\nabla\cdot\mathbf{\Pi} = \nabla p - \eta_s\nabla^2\mathbf{v} - \eta_o\nabla^2(\mathbf{v}\times\hat{\mathbf{z}}). \tag{5}$$

Regarding the electric potential ϕ, we assume the gradual-channel approximation [6,45], i.e., the electric potential is dominated by the gate potential, which effectively screens the Coulomb potential in the long wavelength limit $kd_0 \ll 1$. Thus, the electrostatic force term in Eq. (4) reads

$$\nabla\phi \simeq \frac{ed_0}{\varepsilon_0\varepsilon_r}\nabla n + \frac{ed_0^3}{3\varepsilon_0\varepsilon_r}\nabla\nabla^2 n + \mathcal{O}(d_0^5), \tag{6}$$

where d_0 and $\varepsilon_0\varepsilon_r$ are the thickness and permittivity of the dielectric between the gate and graphene. The second term in the expansion of Eq. (6) gives origin to dispersive corrections of order $\sim d_0/L$ to the plasmon velocity, and the associated effects were described in Ref. [46]. Here, we are interested in long channel devices with strong gate shielding, meaning that $d_0/L \ll 1$; hence, we will retain only the first-order term and drop further corrections. Nonetheless, if desired, the next-order term can be easily incorporated as a rescaling of the Bohm term, since the differential operator has a similar structure.

To consider infinitesimal perturbation along the channel, we linearize Eqs. (3) and (4) around the equilibrium $n = n_0 + n_1 e^{ikx-i\omega t}$, $\mathbf{v} = \mathbf{v}_1 e^{ikx-i\omega t}$, which leads to the dispersion relation

$$\omega = Sk - i\frac{\nu_s}{2}k^2 - \frac{\mathcal{B}/n_0 - \nu_o^2 + (\nu_s/2)^2}{2S}k^3, \tag{7}$$

with $S = \sqrt{e^2d_0n_0/\varepsilon_0\varepsilon_r m_0^\star}$ being the plasmon group velocity and $\nu_{s,o} \equiv \eta_{s,o}/n_0m_0^\star$ the kinematic viscosity. Thus, it is clear that the inclusion of odd viscosity and quantum potential terms does not impact the attenuation of the plasma waves but rather enhances the nonlinearity of the spectrum even in the limit when $\nu_s \ll 1$. The presence of this strong dispersion already hints for the possibility of solitonic solutions, as found in other quantum [47] and relativistic plasmas [48], and as we show in what follows.

III. FINITE AMPLITUDE NONLINEAR WAVES

We start by considering the inviscid limit of the model $\eta_s = \eta_o = 0$ in order to get a better understanding of the Bohm potential effects. Following the approach by Sagdeev [49,50], one can look for one-dimensional traveling wave solutions of Eqs. (3) and (4) by introducing the variable $\xi = x - ct$, with c denoting the wave velocity. This allows us to recast the hydrodynamic equations as

$$-cn' + (nu)' = 0 \tag{8}$$

and

$$-cu' + \left(\frac{u^2}{4} + \frac{v_F^2}{2}\log n + 2S^2\sqrt{\frac{n}{n_0}}\right)' + \frac{\mathcal{B}}{n^{3/2}}(\sqrt{n})''' = 0. \tag{9}$$

Integrating the previous equations once, and imposing the asymptotic conditions $n = n_0$ and $u = 0$ at infinity, one gets the equation of motion governing the density perturbations

$$\mathcal{B}n'' - \frac{3\mathcal{B}}{4n}(n')^2 + n_0^2c^2\left[1 - \frac{n}{n_0} - \log\frac{n}{n_0} + \frac{v_F^2}{2c^2}\left(\frac{n^2}{n_0^2} - 1\right) + \frac{4S^2}{5c^2}\left(\frac{n^{5/2}}{n_0^{5/2}} - 1\right)\right] = 0. \tag{10}$$

The latter can then be multiplied by the quantity $n'/n^{3/2}$ and be integrated once more to reveal the first integral of motion

$$\mathcal{J} = \mathcal{B}\frac{(n')^2}{2n^{3/2}} + \mathcal{V}(n), \tag{11}$$

where $\mathcal{V}$ is the Sagdeev potential

$$\mathcal{V}(n) = \frac{2n_0^2c^2}{\sqrt{n}}\left[1 - \frac{n}{n_0} + \log\frac{n}{n_0} + \frac{v_F^2}{2c^2}\left(\frac{n^2}{3n_0^2} + 1\right) + \frac{4S^2}{5c^2}\left(\frac{n^{5/2}}{4n_0^{5/2}} + 1\right)\right] \tag{12}$$

Moreover, by defining the canonical vector $(q, p) = (n, \mathcal{B}n'/n^{3/2})$, it can be shown that the Hamiltonian

$$H(p, q) = \frac{p^2q^{3/2}}{2\mathcal{B}} + \mathcal{V}(q) \tag{13}$$

retrieves the equation of motion in Eq. (10). Hence, given the form of the pseudopotential $\mathcal{V}$, it is clear that the two-dimensional Hamiltonian flow has two fixed points. One

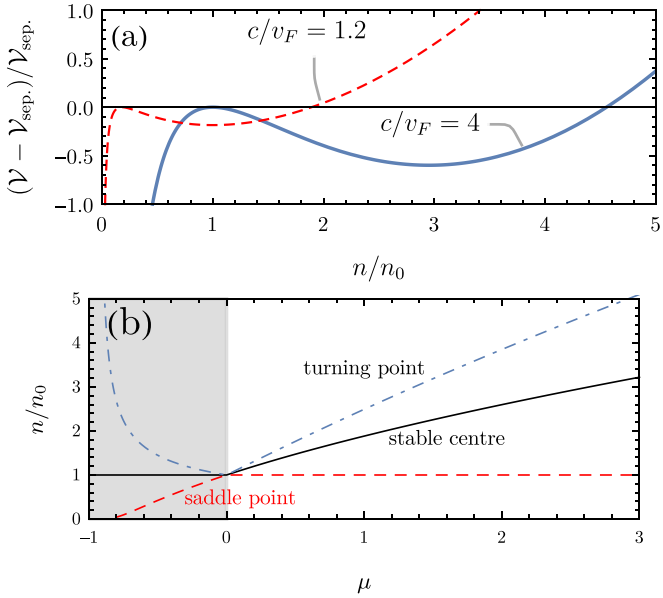

FIG. 1. (a) Pseudopotential from Eq. (12) scaled by its value at the separatrix $\mathcal{V}_{\rm sep.}$ for $\mathcal{B} = 1$, $S/v_F = 2$, and $c/v_F = 4$ (blue solid line) or $c/v_F = 1.2$ (red dashed line). (b) Transcritical bifurcation diagram of Eq. (10), showing the position and nature of the fixed points and the turning point of the separatrix (blue dot-dashed line). The bifurcation swaps the equilibrium (black solid line) and saddle (red dashed line) points.

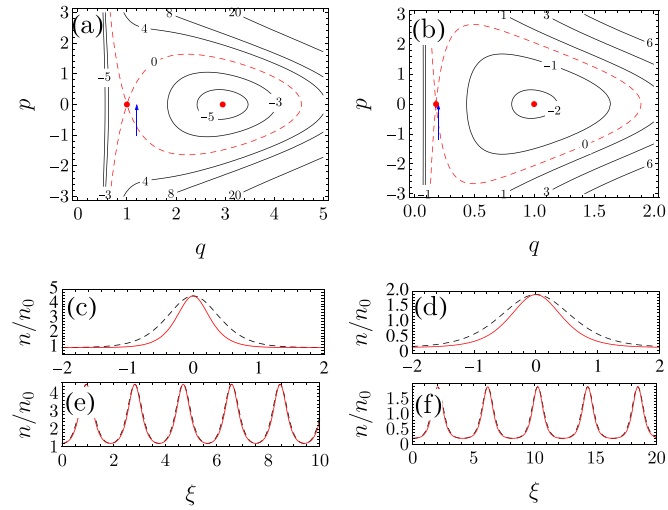

FIG. 2. (a)–(b) Phase space of the Hamiltonian defined in Eq. (13) for $\mathcal{B} = 1$, $S/v_F = 2$, and $c/v_F = 4$ (a) or $c/v_F = 1.2$ (b). The fixed points $(n_0, 0)$ and $(n_c, 0)$ are marked by highlighted dots, and the initial conditions of the oscillatory numerical solutions are indicated by the arrow tip. Bounded orbits exist inside the separatrix (red dashed line). (c)–(f) Numerical solutions of orbits on the phase space. The solitary (c)–(d) and oscillatory (e)–(f) numerical solutions (red solid line) are compared against cnoidal analytical expressions of the same amplitude and wavelength (black dashed line).

located at $(q, p) = (n_0, 0)$ independently of the model parameters, besides mean density, and a second point wandering along the q axis $(q, p) = (n_c, 0)$, where n_c is a function of the model parameters. Such two points undergo a transcritical saddle-center bifurcation governed by the parameter $\mu = c^2/(S^2 + v_F^2/2) - 1$ as made evident by Fig. 1, where we can see the fixed points colliding and swapping their nature. Furthermore, the position of the mobile fixed point is taken to be, up to first order, $n_c/n_0 \approx c^2/(S^2 + v_F^2/2)$. The nature of this bifurcation ensures persistence of the stable center and saddle pair, and thus one can deduce the occurrence of nonlinear oscillations around the center point, provided that the Hamiltonian level is lower than that of the saddle point, which defines the separatrix, i.e., $\Delta H = H - H_{\rm separatrix} < 0$. Figure 2 illustrates the phase space of the system showing the stable region enclosed by the separatrix. It is evident that the system sustains nonlinear oscillations around the stable center point. Those are similar to cnoidal waves although, in fact, not elliptic functions, given the nonrational nature of the potential $\mathcal{V}(q)$. Yet, the soliton solutions that live along the separatrix are more narrow than the usual profile. Moreover, it is interesting to note that, while for $\mu > 0$ the soliton amplitude scales as $A \sim \mu \sim c^2$, in the case of $\mu < 0$, i.e., for the slow solitons, the amplitude strongly deviates from the linearity on μ (cf. Fig. 1). Particularly in the limit of $c \to 0$ we have $A \sim \mu^{-3/2}$.

The possibility to maintain and propagate solitary waves of substantial amplitude can be exploited to transmit pulsed signals along a graphene channel. However, to accommodate the dissipative effects on the analysis, we must resort to perturbative methods.

IV. SMALL AMPLITUDE NONLINEAR WAVES

Although finite amplitude waves can be excited in the studied inviscid regime, the inclusion of viscous effects is central to a more faithful description of nonlinear waves in Dirac electronic fluids. In this section we will deal with the viscosities, both shear and odd, and with the dynamics in the transverse direction; to do so, we will now restrict ourselves to waves in the perturbative regime.

The general procedure to implement the reductive perturbation method (RPM) [51–54] starts with casting the model Eqs. (3) and (4) in a general quasilinear form

$$\left[\frac{\partial}{\partial t} + \mathbf{A}^x\frac{\partial}{\partial x} + \mathbf{A}^y\frac{\partial}{\partial y} + \mathbf{K}\left(\frac{\partial^2}{\partial x^2} + \frac{\partial^2}{\partial y^2}\right) + \mathbf{H}^x\left(\frac{\partial^3}{\partial x^3} + \frac{\partial^3}{\partial x\partial y^2}\right)\right]\mathbf{U} = 0, \tag{14}$$

with the state vector $\mathbf{U} = (n, u, v)^T$ and the matrices

$$\mathbf{A}^x = \begin{pmatrix} u & n & 0 \\ \frac{S^2}{\sqrt{n_0 n}} & \frac{u}{2} & 0 \\ 0 & -\frac{v}{2} & u \end{pmatrix}, \quad \mathbf{A}^y = \begin{pmatrix} v & 0 & n \\ 0 & v & -\frac{u}{2} \\ \frac{S^2}{\sqrt{n_0 n}} & 0 & \frac{v}{2} \end{pmatrix}$$

$$\mathbf{K} = \begin{pmatrix} 0 & 0 & 0 \\ 0 & -\nu_s & -\nu_o \\ 0 & \nu_o & -\nu_s \end{pmatrix}, \quad \mathbf{H}^x = \frac{\mathcal{B}}{2n_0^2}\begin{pmatrix} 0 & 0 & 0 \\ 1 & 0 & 0 \\ 1 & 0 & 0 \end{pmatrix}. \tag{15}$$

In the derivation of Eq. (15), we dropped the Fermi pressure. This approximation is justified since the electrostatic force dominates over Fermi pressure as $S^2/v_F^2 \gg 1$ in most scenarios. Also, the inclusion of the Fermi pressure would simply translate to a redifinition of the wave velocity at linear order.

Moreover, we linearized the Bohm term; in fact, only the zeroth order of $\mathbf{H}^x$ plays a role in the RPM as will become evident in what follows.

A. Dissipative Kadomtsev-Petviashvili equation

Performing a Gardiner-Morikawa transformation [53,54] on Eq. (14), with the introduction of the set of stretched variables

$$\begin{aligned}\xi &= \epsilon^{1/2}(x-\lambda t),\\ \zeta &= \epsilon y, \text{ and}\\ \tau &= \epsilon^{3/2} t,\end{aligned} \tag{16}$$

where ϵ is a small perturbation parameter being also used for the expansion of the variables

$$\begin{aligned}n &= n_0 + \epsilon n_1 + \epsilon^2 n_2 + \cdots\\ u &= \epsilon u_1 + \epsilon^2 u_2 + \cdots\\ v &= \epsilon^{3/2} v_1 + \epsilon^{5/2} v_2 + \cdots\end{aligned} \tag{17}$$

as well as for the matrices, e.g., $\mathbf{A}^x = \mathbf{A}^x_0 + \epsilon \mathbf{A}^x_1 + \cdots$ and so on. The choice of the exponents of ϵ is such that propagation along x is predominant, and the dispersion relation Eq. (7) remains invariant. Additionally, in order to capture the effect of the dissipation of the second term on the RHS of Eq. (7), the shear viscosity must also be scaled as $\nu_s = \epsilon^{1/2}\tilde{\nu}_s$.

Moreover, in the context of the RPM, we can introduce the first-order perturbation field φ such that

$$\mathbf{U}_1 = (\pm n_0/S, 1, 0)^T \varphi, \tag{18}$$

where the plus and minus sign refer to right or left propagating waves, respectively, and then we can derive a dissipative generalization of the Kadomtsev-Petviashvili (KP) [55] equation (see Appendix 1)

$$\frac{\partial}{\partial\xi}\left(\frac{\partial\varphi}{\partial\tau} + \frac{3\pm1}{4}\varphi\frac{\partial\varphi}{\partial\xi} - \frac{\tilde{\nu}_s}{2}\frac{\partial^2\varphi}{\partial\xi^2} \pm \frac{\mathcal{B}/n_0 - v_o^2}{2S}\frac{\partial^3\varphi}{\partial\xi^3}\right) \pm \frac{S}{2}\frac{\partial^2\varphi}{\partial\zeta^2} = 0, \tag{19}$$

akin to what is found in the literature for other quantum plasmas [56–58].

In the one-dimensional limit of Eq. (19) one retrieves a dissipative generalization of the well-known Kortweg–de Vries–Burgers (KdVB) equation

$$\frac{\partial\varphi}{\partial\tau} + \frac{3\pm1}{4}\varphi\frac{\partial\varphi}{\partial\xi} - \frac{\tilde{\nu}_s}{2}\frac{\partial^2\varphi}{\partial\xi^2} \pm \frac{\mathcal{B}/n_0 - v_o^2}{2S}\frac{\partial^3\varphi}{\partial\xi^3} = 0. \tag{20}$$

This equation admits both oscillatory and shock-type solutions [59–61]. While the traveling shocks may be valuable for signal propagation engineering schemes, the oscillatory modes may trigger instabilities that could, in future technological applications, be harnessed to excite radiative emission.

Regarding the instance of unstable modes, let us devote our attention to right-propagating solutions, setting $\chi = \xi - c\tau$ as independent variable, Eq. (20) can be cast to the dimensionless form

$$-\varphi' + \varphi\varphi' - \varepsilon\varphi'' + \beta\varphi''' = 0, \tag{21}$$

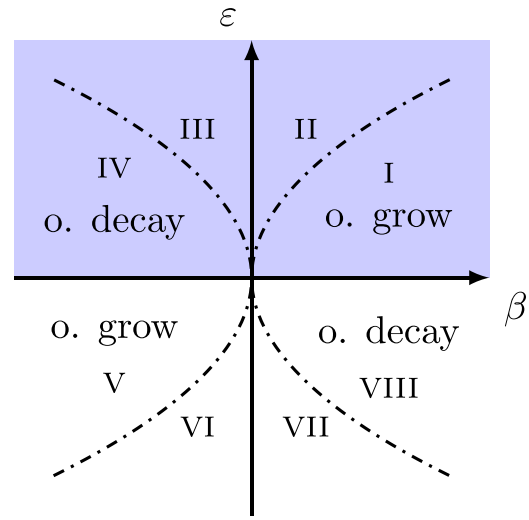

FIG. 3. Parameter space regions with distinct qualitative behavior, bounded by $\varepsilon^4 = 16\beta^2$. Regions II, III, VI, and VII only sustain bounded solutions along the heteroclinic orbit connecting the two fixed points. Whilst the remaining areas (labeled with o.) feature oscillatory solutions, either decaying or growing in time. Shaded region $\varepsilon \geqslant 0$ indicating the achievable region of positive shear viscosity.

with

$$\varepsilon \equiv \frac{\tilde{\nu}_s}{2cL} \quad \text{and} \quad \beta \equiv \frac{\mathcal{B}/n_0 - v_o^2}{2ScL^2}, \tag{22}$$

such that the global stability and qualitative behavior of Eq. (21) can be analyzed in terms of such parameters, as we show below. Integration of Eq. (21) yields

$$-\varphi + \tfrac{1}{2}\varphi^2 - \varepsilon\varphi' + \beta\varphi'' = r, \tag{23}$$

with r being an integration constant. Requiring the perturbation field to vanish at infinity, we set $r = 0$. As such, the flow linearization around the fixed points of Eq. (23), to wit,

$$(\varphi_-, \varphi'_-) = (0, 0) \quad \text{and} \quad (\varphi_+, \varphi'_+) = (2, 0), \tag{24}$$

yields the eigenvalues

$$\lambda_{1,2}(\varphi_-) = \frac{\varepsilon \pm \sqrt{\varepsilon^2 + 4\beta}}{2\beta} \text{ and} \tag{25}$$

$$\lambda_{1,2}(\varphi_+) = \frac{\varepsilon \pm \sqrt{\varepsilon^2 - 4\beta}}{2\beta}. \tag{26}$$

As consequence, the global behavior of the dynamical system can be categorized by the regions bounded by $\varepsilon^2 \pm 4\beta = 0$ as illustrated in Fig. 3, while the behavior of the fixed points is listed in Table I.

Equation (21) can be seen as a combination of KdV and Burger's equations and, indeed, its solutions present a crossover between the characteristic solutions of either KdV and Burger's, corresponding to the limits of negligible viscosity or dispersion, respectively.

Notably, for regions I, IV, V, and VIII, i.e., $|\beta| > \varepsilon^2/4$ the eigenvalues of one of the fixed points are complex conjugates, leading to stable (region IV) or unstable (region I) spirals. And, even though the presence of viscosity breaks the homoclinic orbit, the system sustains oscillatory solutions, either

TABLE I. Schematic diagrams and behavior of the phase portrait of Kortweg–de Vries–Burgers equation [Eq. (23)] around the fixed points for the regions of parameters I through VIII.

Region	Phase Portrait	Behavior φ_-	Behavior φ_+
I		saddle	unstable spiral
II		saddle	unstable node
III		stable node	saddle
IV		stable spiral	saddle
V		unstable spiral	saddle
VI		unstable node	saddle
VII		saddle	stable node
VIII		saddle	stable spiral

decaying or increasing in time (cf. Fig. 4). For longer times, the self-growing modes will either collide with the hyperbolic point, reaching a local equilibrium, or not being able to support themselves indefinitely and the nonlinear effects of the next order terms (that is, the response of n_2, u_2 and so on) will lead to the saturation or collapse of the wave. Nonetheless, even if short-lived, these modes can be used to trigger or reinforce other wave instabilities.

Further, for $|\beta| < \varepsilon^2/4$, as all eigenvalues are real, the only bounded solutions are those advancing on the heteroclinic orbit $\varphi' = (\varphi^2/2 - \varphi)/\varepsilon$ connecting the fixed points. Consequently, the allowed solutions are sigmoidlike shock waves, similar to the solutions of Burger's equation. In particular, for $|\beta| = 6\varepsilon^2/25$ there is an analytical solution [62,63] in the form $\frac{8}{3}(1 + e^{(\xi - c\tau - C_1)/\sqrt{6}})^{-2}$, for other values of the ratio β/ε^2 the numerical solutions follow a similar profile.

It has been argued in Ref. [64] that only the shock solutions can have physical significance, the reasoning being that in the common scenarios—often astrophysical ones—the parameters of KdVB equation are not independent. However, in our system the coefficients are determined by a variety of physical parameters that can be set independently, viz., permittivity and thickness of the dielectric, Fermi level of the carriers, and both viscosities.

B. Modulational instability and nonlinear Schrödinger equation

So far in this work, we considered only unmagnetized scenarios, where the quantum correction of the Bohm potential is crucial for the dispersive behavior of the waves. However, in the presence of a magnetic field, the onset of the cyclotron frequency (ω_c) gap in the dispersion relation causes the magnetic effects to dominate over those of the quantum potential. Therefore, we will now drop the Bohm contribution and focus on the nonlinear effects under a magnetic field.

Introducing a weak magnetic field [29] to the model, with the addition of a $\omega_c \mathbf{v} \times \hat{\mathbf{z}}$ source term in Eq. (4), leads to yet another nonlinear behavior: the emergence of modulational instability. Indeed, from the hydrodynamic model written as

$$\left[\frac{\partial}{\partial t} + \mathbf{A}\frac{\partial}{\partial x} + \mathbf{K}\frac{\partial^2}{\partial x^2} + \mathbf{B}\right]\mathbf{U} = 0, \tag{27}$$

we can obtain the dispersion relation

$$\omega^2 = \omega_c^2 + S^2k^2 + \nu_o^2k^4 - 2\nu_o\omega_c k^2. \tag{28}$$

Then, following once again the prescription of the reductive perturbation method, now for the wave amplitude envelope

$$\mathbf{U} = \mathbf{U}_0 + \sum_{\substack{p=1 \\ |\ell| \leqslant p}}^{\infty} \epsilon^p \mathbf{U}_p^{(\ell)} e^{-i\ell(\omega t - kx)}, \tag{29}$$

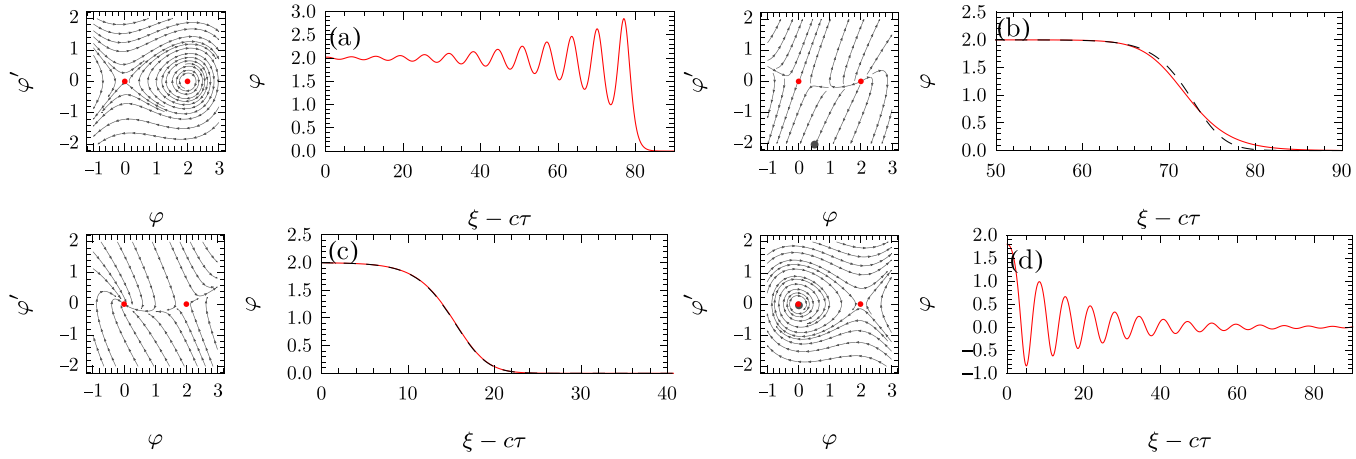

FIG. 4. Phase space (left, streamline plots) and numerical solutions (right, red solid line) of Eq. (21) for the positive viscosity regions, showing: (a) the growing oscillations $\varepsilon = 0.1$, $\beta = 1$, (b) shock propagation $\varepsilon = 0.1$, $\beta = 1$, (c) idem $\varepsilon = 5/\sqrt{6}$, $\beta = -1$, (d) decaying oscillations $\varepsilon = 0.1$, $\beta = -1$. On panel (c) the analytical solution is superimposed (black dashed line) and on (b) a solution of the same form is also plotted for comparison. At the phase space plots the fixed points ($\varphi_\pm$, $\varphi'_\pm$) are highlighted (red dots).

and defining the scalar ψ from the first harmonic of the first-order term and the appropriate right eigenvector of the differential operator of Eq. (27), i.e., $\mathbf{U}_1^{(1)} \equiv (n_0, \pm\omega/k, i(k^2\nu_o - \omega_c)/k)^T\psi$, one can derive (see Appendix 2 for details) a nonlinear Schrödinger equation (NLSE) for the perturbation field, in the form

$$i\frac{\partial\psi}{\partial\tau} + \frac{\omega''}{2}\frac{\partial^2\psi}{\partial\xi^2} + Q|\psi|^2\psi = 0, \tag{30}$$

where $\omega'' \equiv \partial^2\omega/\partial k^2$ and Q the Kerr-like nonlinear term which can be cast as

$$Q = \frac{q(\omega, \omega_c, S, \nu_o)}{48n_0^2\omega\omega_c\left(4k^4\nu_o^2 - \omega_c^2\right)}, \tag{31}$$

with q a somewhat complex polynomial given by

$$\begin{aligned} q(\omega, \omega_c, S, \nu_o) = &-4\omega_c\left(11\omega^4 + 9\omega^2\omega_c^2 - 8\omega_c^4\right) + k^2\left[S^2\omega_c\left(4\omega^2 + 177\omega_c^2\right) + 16\nu_o\left(3\omega^4 + 3\omega^2\omega_c^2 - 20\omega_c^4\right)\right] \\ &+ 4k^4\left[26S^4\omega_c + 3S^2\nu_o\left(4\omega^2 - 57\omega_c^2\right) + 3\nu_o^2\omega_c\left(7\omega^2 + 96\omega_c^2\right)\right] \\ &- 4k^6\nu_o\left[24S^4 - 231S^2\nu_o\omega_c + 8\nu_o^2\left(3\omega^2 + 58\omega_c^2\right)\right] + 32k^8\nu_o^3(43\nu_o\omega_c - 15S^2) - 384k^{10}\nu_o^5, \end{aligned} \tag{32}$$

where the wave vector k is implicitly given by Eq. (28).

Such NLSE is known to foster the development of modulational instability [53,65]. For the system to be unstable to modulations, it must comply with the Lighthill criterion $\omega''Q > 0$, i.e., to be *self-focusing* [66]. Since for small ν_o the dispersion relation Eq. (28) ensures $\omega'' > 0$ the region of instability is determined by Q alone; in fact, there is a region of parameters that leads to instability, as can be seen in Fig. 5. In that case, the spectral sidebands of a signal propagating in the system will grow, and the signal will increasingly modulate. Furthermore, in the limit of infinite wavelength of the modulation, the system can transmit a wave packet with an envelope governed by Eq. (30), i.e., a Peregrine soliton [67,68], similarly to the situation in optical media where this type of instability is well known and exploited.

V. CONCLUSION

The hydrodynamics of charged carriers on graphene has significant differences from regular fluid description of a two-dimensional electron gas, notably the local Drude mass, meaning that $m^\star(x,t) \propto \sqrt{n(x,t)}$, and the Bohm potential. As they enhance the dispersive nature of the flow, they favor the formation of nonlinear waves. We studied two classes of nonlinear waves: finite amplitude waves and perturbative waves. The former arises from a Sagdeev pseudopotential approach, while the latter stems from a reductive perturbative method that yields a generalized Kadomtsev-Petviashvili equation.

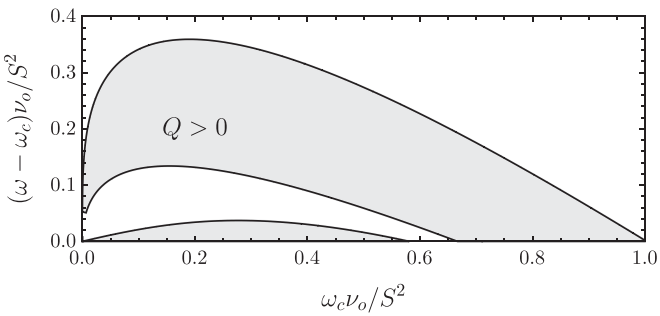

FIG. 5. Region of instability for the nonlinear Schrödinger equation, Eq. (30). In the shaded regions, the positive Kerr term leads to a self-focusing (unstable) mode.

In the case of waves of general amplitude (although restricted to high Reynolds numbers), our findings reveal interesting properties: (i) the formation of cnoidal-like waves that are not given in terms of elliptic functions, (ii) the formation of solitons, propagating both above and below the group velocity of the linear plasmons. Remarkably, the latter violate the usual amplitude-velocity relation obtained for solitons within the Kortweg–de Vries description [69]. In the perturbative scenario, the reduction of Kadomtsev-Petviashvili equation to the Kortweg–de Vries–Burgers equation exhibits regions of parameters for which oscillating shock waves are formed. In effect, the numerical solutions denote the transition between the viscosity dominated regime—in which the solutions are pure (nonoscillatory) shocks—and the low viscosity case, for which nonlinear oscillations, akin to the ones from Kortweg–de Vries equation, superimposed with the shock profile are found. Furthermore, we extended the perturbative analysis of the magnetized case, retrieving a nonlinear Schrödinger equation and showing the presence of modulational instability near the cyclotronic resonance.

All the above points to the possible emergence of rather interesting nonlinear states, in particular propagating shock waves and solitons that can be exploited for plasmonic signal transmission along future graphene wave guides and circuitry. Moreover, the oscillatory unstable modes have the potential to drive the emission of radiation or to prompt even further unstable modes that we have not yet considered in our analysis, such as thermal instabilities and shock instabilities. Conversely, it is also foreseeable that the nonlinear effects described by our depiction will respond to external stimuli like radiation and temperature gradients, for instance. Therefore, they may prove useful also for sensing applications.

ACKNOWLEDGMENTS

The authors acknowledge Fundação para a Ciência e a Tecnologia (FCT-Portugal) through Contract No. CEECIND/00401/2018, through the Project No. PTDC/FIS-OUT/3882/2020, the Exploratory Project No.

UTA-EXPL/NPN/0038/2019, and through the Grant No. PD/BD/150415/2019.

APPENDIX: REDUCTIVE PERTURBATION METHOD

1. Dissipative Kadomtsev-Petviashvili

The general procedure to implement the reductive perturbation method [51–54] starts with recasting the model Eqs. (3) and (4) in the general quasilinear form of Eq. (14), with the state vector $\mathbf{U} = (n, u, v)^T$ and the matrices defined in Eq. (15). Then, one performs a Gardiner-Morikawa transformation introducing the set of stretched variables [53,54]

$$\begin{aligned} \xi &= \epsilon^{1/2}(x - \lambda t), \\ \zeta &= \epsilon y, \text{ and} \\ \tau &= \epsilon^{3/2} t, \end{aligned} \tag{A1}$$

with ϵ being the small perturbation parameter being also used for the expansion of the variables, as well as for the matrices, e.g., $\mathbf{A}^x = \mathbf{A}_0^x + \epsilon \mathbf{A}_1^x + \cdots$ and so on. Additionally, the shear viscosity must also be scaled as $\eta_s = \epsilon^{1/2}\tilde{\eta}_s$ and so the matrix $\mathbf{K}$ must be split as $\mathbf{K} = \mathbf{K}_o + \epsilon^{1/2}\mathbf{K}_s$.

Expanding Eq. (14) as stated, and equating each coefficient of the ϵ expansion to zero yields, at the lowest order $\epsilon^{3/2}$,

$$\left(\mathbf{A}_0^x - \lambda\right)\frac{\partial}{\partial \xi}\mathbf{U}_1 = 0, \tag{A2}$$

while at the next order ϵ^2

$$\left(\mathbf{A}_0^x - \lambda\right)\frac{\partial}{\partial \xi}\mathbf{U}_{3/2} + \left(\mathbf{A}_0^y \frac{\partial}{\partial \zeta} + \mathbf{K}_o \frac{\partial^2}{\partial \xi^2}\right)\mathbf{U}_1 = 0, \tag{A3}$$

and finally, at order $\epsilon^{5/2}$

$$\begin{aligned} &\left(\mathbf{A}_0^x - \lambda\right)\frac{\partial}{\partial \xi}\mathbf{U}_2 + \left(\mathbf{A}_0^y \frac{\partial}{\partial \zeta} + \mathbf{K}_o \frac{\partial^2}{\partial \xi^2}\right)\mathbf{U}_{3/2} \\ &\quad + \left(\frac{\partial}{\partial \tau} + \mathbf{A}_1^x \frac{\partial}{\partial \xi} + \mathbf{K}_s \frac{\partial^2}{\partial \xi^2} + \mathbf{H}_0^x \frac{\partial^3}{\partial \xi^3}\right)\mathbf{U}_1 = 0. \end{aligned} \tag{A4}$$

To simplify the previous equations, let the right and left eigenvectors of $\mathbf{A}_0^x$ associated with the eigenvalue λ be defined as $\mathbf{L}_1$ and $\mathbf{R}_1$. Then, Eq. (A2) will be automatically satisfied if there is a scalar φ that captures the time and spatial evolution, such that

$$\mathbf{U}_1 = \varphi \mathbf{R}_1. \tag{A5}$$

Moreover, by multiplying Eq. (A4) by $\mathbf{L}_1$ on the left, the first term cancels, therefore yielding

$$\begin{aligned} &\mathbf{L}_1\mathbf{R}_1 \frac{\partial \varphi}{\partial \tau} + \mathbf{L}_1\mathbf{A}_1^x\mathbf{R}_1 \frac{\partial \varphi}{\partial \xi} + \mathbf{L}_1\mathbf{K}_s\mathbf{R}_1 \frac{\partial^2 \varphi}{\partial \xi^2} + \mathbf{L}_1\mathbf{H}_0^x\mathbf{R}_1 \frac{\partial^3 \varphi}{\partial \xi^3} \\ &\quad = -\mathbf{L}_1\left(\mathbf{A}_0^y \frac{\partial}{\partial \zeta} + \mathbf{K}_o \frac{\partial^2}{\partial \xi^2}\right)\mathbf{U}_{3/2}, \end{aligned} \tag{A6}$$

where we also made use of Eq. (A5), and Eq. (A3) can now be used to simplify the RHS of the latter.

2. Nonlinear Schrödinger equation

To derive the nonlinear Schrödinger equation (NLSE) from the fluid equations we will, once again, cast the system on its quasilinear form given by Eq. (27). We limit the discussion to the case of one-dimensional propagation, and discard the quantum potential. Also, we only allow for linear source and diffusion terms, i.e., $\mathbf{B} \equiv \mathbf{B}_0$ and $\mathbf{K} \equiv \mathbf{K}_0$, as defined in the expansion prescription discussed in the previous section. For our hydrodynamic model, we have

$$\begin{aligned} \mathbf{A} &= \begin{pmatrix} u & n & 0 \\ \frac{S^2}{\sqrt{n_0 n}} & \frac{u}{2} & 0 \\ 0 & -\frac{v}{2} & u \end{pmatrix}, \quad \mathbf{K} = \begin{pmatrix} 0 & 0 & 0 \\ 0 & -\nu_s & -\nu_o \\ 0 & \nu_o & -\nu_s \end{pmatrix} \\ \mathbf{B} &= \begin{pmatrix} 0 & 0 & 0 \\ 0 & 0 & -\omega_c \\ 0 & \omega_c & 0 \end{pmatrix}. \end{aligned} \tag{A7}$$

We now expand the wave amplitude envelope as

$$\mathbf{U} = \mathbf{U}_0 + \sum_{p=1}^{\infty} \epsilon^p \mathbf{U}_p = \mathbf{U}_0 + \sum_{\substack{p=1 \\ |\ell| \leqslant p}}^{\infty} \epsilon^p \mathbf{U}_p^{(\ell)} e^{-i\ell(\omega t - kx)}, \tag{A8}$$

and notice that $\mathbf{U}$ is a real vector $\mathbf{U}_p^{(-\ell)} \equiv \mathbf{U}_p^{(\ell)*}$. Also, we expand the matrix $\mathbf{A}$ as

$$\begin{aligned} \mathbf{A} = \mathbf{A}_0 + \sum_{p=1}^{\infty} \epsilon^p \mathbf{A}_p &= \mathbf{A}_0 + \epsilon \mathbf{A}'[U_1] \\ &\quad + \epsilon^2(\mathbf{A}'[U_2] + \mathbf{A}''[U_1 U_1]) + \cdots, \end{aligned} \tag{A9}$$

where we used the following notation

$$\mathbf{A}'[X] \equiv \frac{\partial \mathbf{A}}{\partial u_k} X_k = \frac{\partial A_{ij}}{\partial u_k} X_k, \tag{A10}$$

$$\mathbf{A}''[XY] \equiv \frac{1}{2}\frac{\partial^2 \mathbf{A}}{\partial u_k \partial u_m} X_k Y_m = \frac{1}{2}\frac{\partial^2 A_{ij}}{\partial u_k \partial u_m} X_k Y_m. \tag{A11}$$

Making use of the previous expansions and collecting the terms of Eq. (27), which are of order ϵ, we have

$$\sum_{\ell} \mathbf{W}_0^{(\ell)} \mathbf{U}_1^{(\ell)} e^{i\ell\vartheta} = 0, \tag{A12}$$

with

$$\mathbf{W}_0^{(\ell)} = -i\ell\omega \mathbf{I} + i\ell k \mathbf{A}_0 - \ell^2 k^2 \mathbf{K}_0 + \mathbf{B}_0. \tag{A13}$$

The right eigenvector of the first mode is used to scale the first-order perturbation, introducing the scalar ψ satisfying the following equivalence

$$\mathbf{W}_0^{(1)} \mathbf{U}_1^{(1)} = 0 \iff \mathbf{W}_0^{(1)} \mathbf{R}_1^{(1)} \psi = 0. \tag{A14}$$

Likewise, the second order $\sim\epsilon^2$ terms lead to

$$\begin{aligned} &\sum_{\ell} \left(\mathbf{W}_0^{(\ell)} \mathbf{U}_2^{(\ell)} + (\mathbf{A}_0 - \lambda \mathbf{I} + 2i\ell k \mathbf{K}_0)\frac{\partial \mathbf{U}_1^{(\ell)}}{\partial \xi}\right) e^{i\ell\vartheta} \\ &\quad + \sum_{\ell', m} i\ell' k \mathbf{A}'\left[U_1^{(m)}\right] \mathbf{U}_1^{(\ell')} e^{i(\ell' + m)\vartheta} = 0, \end{aligned} \tag{A15}$$

which, when equating the modes ℓ and $\ell' + m$, yield the following relations

$$\mathbf{U}_2^{(0)} = \mathbf{R}_2^{(0)} |\psi|^2, \quad \mathbf{U}_2^{(1)} = \mathbf{R}_2^{(1)} \frac{\partial \psi}{\partial \xi}, \quad \text{and} \quad \mathbf{U}_2^{(2)} = \mathbf{R}_2^{(2)} \psi^2, \tag{A16}$$

with $\mathbf{R}_2^{(\ell)}$ vectors given by

$$\begin{aligned}
\mathbf{R}_2^{(0)} &\equiv -ik\mathbf{W}_0^{(0)^{-1}}\left(\mathbf{A}'\left[R_1^{(1)*}\right]\mathbf{R}_1^{(1)} - \mathbf{A}'\left[R_1^{(1)}\right]\mathbf{R}_1^{(1)*}\right),\\
\mathbf{R}_2^{(1)} &\equiv -\mathbf{W}_0^{(1)^{-1}}(\mathbf{A}_0 - \boldsymbol{\lambda} + 2i\ell k\mathbf{K}_0)\mathbf{R}_1^{(1)},\\
\mathbf{R}_2^{(2)} &\equiv -ik\mathbf{W}_0^{(2)^{-1}}\mathbf{A}'\left[R_1^{(1)}\right]\mathbf{R}_1^{(1)}.
\end{aligned} \tag{A17}$$

Finally, at order ϵ^3 we get

$$\begin{aligned}
&\sum_\ell \left(\mathbf{W}_0^{(\ell)}\mathbf{U}_3^{(\ell)} + \frac{\partial \mathbf{U}_1^{(\ell)}}{\partial\tau} + \mathbf{K}_0\frac{\partial^2\mathbf{U}_1^{(\ell)}}{\partial\xi^2}\right.\\
&\quad\left. + (\mathbf{A}_0 - \boldsymbol{\lambda}\mathbf{I} + 2i\ell k\mathbf{K}_0)\frac{\partial\mathbf{U}_2^{(\ell)}}{\partial\xi}\right)e^{i\ell\vartheta}\\
&\quad + \sum_{\ell',m}\left(ik\ell'\mathbf{A}'\left[U_1^{(m)}\right]\mathbf{U}_2^{(\ell')} + \mathbf{A}'\left[U_1^{(m)}\right]\frac{\partial\mathbf{U}_1^{(\ell')}}{\partial\xi}\right)e^{i(\ell'+m)\vartheta}\\
&\quad + \sum_{l,j,n} ilk\mathbf{A}'\left[U_2^{(j)}\right]\mathbf{U}_1^{(l)}e^{i(l+j)\vartheta}\\
&\quad + ilk\mathbf{A}''\left[U_1^{(j)}U_1^{(n)}\right]\mathbf{U}_1^{(l)}e^{i(l+j+n)\vartheta} = 0,
\end{aligned} \tag{A18}$$

and collecting the first-mode ($\ell = 1$) terms, one gets

$$\begin{aligned}
&\mathbf{W}_0^{(1)}\mathbf{U}_3^{(1)} + \mathbf{R}_1^{(1)}\frac{\partial\psi}{\partial\tau} + \mathbf{K}_0\mathbf{R}_1^{(1)}\frac{\partial^2\psi}{\partial\xi^2}\\
&\quad + (\mathbf{A}_0 - \boldsymbol{\lambda} + 2ik\mathbf{K}_0)\mathbf{R}_2^{(1)}\frac{\partial^2\psi}{\partial\xi^2}\\
&\quad \times i2k\mathbf{A}'\left[R_1^{(-1)}\right]\mathbf{R}_2^{(2)}\psi^*\psi^2 + ik\mathbf{A}'\left[R_2^{(0)}\right]\mathbf{R}_1^{(1)}|\psi|^2\psi\\
&\quad - ik\mathbf{A}'\left[R_2^{(2)}\right]\mathbf{R}_1^{(-1)}\psi^2\psi^* - ik\mathbf{A}''\left[R_1^{(1)}R_1^{(1)}\right]\mathbf{R}_1^{(-1)}\psi\psi\psi^*\\
&\quad + 2ik\mathbf{A}''\left[R_1^{(1)}R_1^{(-1)}\right]\mathbf{R}_1^{(1)}\psi\psi^*\psi = 0.
\end{aligned} \tag{A19}$$

By multiplying Eq. (A19) by $i\mathbf{L}_1^{(1)}$, such that $\mathbf{L}_1^{(1)}\mathbf{W}_0^{(1)} = 0$, we arrive to

$$\begin{aligned}
&i\mathbf{L}_1^{(1)}\mathbf{R}_1^{(1)}\frac{\partial\psi}{\partial\tau} + i\mathbf{L}_1^{(1)}\left[\mathbf{K}_0\mathbf{R}_1^{(1)} + (\mathbf{A}_0 - \lambda\mathbf{I} + 2ik\mathbf{K}_0)\mathbf{R}_2^{(1)}\right]\frac{\partial^2\psi}{\partial\xi^2}\\
&\quad - k\mathbf{L}_1^{(1)}\left(2\mathbf{A}'\left[R_1^{(1)*}\right]\mathbf{R}_2^{(2)} - \mathbf{A}'\left[R_2^{(2)}\right]\mathbf{R}_1^{(1)*} + \mathbf{A}'\left[R_0^{(2)}\right]\mathbf{R}_1^{(1)}\right.\\
&\quad \left. + 2\mathbf{A}''\left[R_1^{(1)}R_1^{(1)*}\right]\mathbf{R}_1^{(1)} - \mathbf{A}''\left[R_1^{(1)}R_1^{(1)}\right]\mathbf{R}_1^{(1)*}\right)|\psi|^2\psi = 0,
\end{aligned} \tag{A20}$$

which can be read as a nonlinear Schrödinger equation,

$$i\frac{\partial\psi}{\partial\tau} + \frac{1}{2}\omega''\frac{\partial^2\psi}{\partial\xi^2} + Q|\psi|^2\psi = 0. \tag{A21}$$

To retrieve the instability criterion and associated growth rate, one can resort to the ansatz $\psi = (\sqrt{P_0} + a(\xi,\tau))e^{iQP_0\tau}$, where $a(\xi,\tau) = c_1e^{i(\kappa\xi-\Omega\tau)} + c_2e^{-i(\kappa\xi-\Omega\tau)}$. This leads to the dispersion relation

$$\Omega^2 = \left(\frac{\omega''}{2}\right)^2\kappa^4 - 2\left(\frac{\omega''}{2}\right)QP_0\kappa^2, \tag{A22}$$

for the modulation frequency Ω and wave number κ. The instability condition requires $\omega''Q > 0$, and the unstable modes satisfy the condition $\kappa^2 < 2Q/\omega''$. It can also be shown that the maximum growth rate $\gamma_{\max} \equiv \max_\kappa \Im\Omega(\kappa) = QP_0$, proportional to the Kerr nonlinear term Q.

[1] C. Wang, X. Duan, and X. Duan, in *2D Materials*, edited by P. Avouris, T. F. Heinz, and T. Low (Cambridge University Press, Cambridge, 2017) pp. 159–179

[2] R. Murali, in *Graphene Nanoelectronics*, edited by R. Murali (Springer US, Boston, MA, 2012) pp. 51–91.

[3] S. Chung, R. A. Revia, and M. Zhang, Adv. Mater. **33**, 1904362 (2021).

[4] L. Sun, L. Huang, Y. Wang, Y. Lian, G. Huang, H. Zhao, and K. Zheng, IEEE Photon. J. **13**, 1 (2021).

[5] V. Mitin, T. Otsuji, and V. Ryzhii, eds., *Graphene-Based Terahertz Electronics and Plasmonics* (Jenny Stanford Publishing, 2020), Vol. 148, pp. 148–162.

[6] A. Tomadin and M. Polini, Phys. Rev. B **88**, 205426 (2013).

[7] L. F. Man, W. Xu, Y. M. Xiao, H. Wen, L. Ding, B. Van Duppen, and F. M. Peeters, Phys. Rev. B **104**, 125420 (2021).

[8] R. Toshio and N. Kawakami, Phys. Rev. B **106**, L201301 (2022).

[9] A. Lucas and K. C. Fong, J. Phys.: Condens. Matter **30**, 053001 (2018).

[10] B. N. Narozhny, Ann. Phys. **411**, 167979 (2019).

[11] M. Müller, J. Schmalian, and L. Fritz, Phys. Rev. Lett. **103**, 025301 (2009).

[12] M. J. H. Ku, T. X. Zhou, Q. Li, Y. J. Shin, J. K. Shi, C. Burch, L. E. Anderson, A. T. Pierce, Y. Xie, A. Hamo, U. Vool, H. Zhang, F. Casola, T. Taniguchi, K. Watanabe, M. M. Fogler, P. Kim, A. Yacoby, and R. L. Walsworth, Nature (London) **583**, 537 (2020).

[13] J. A. Sulpizio, L. Ella, A. Rozen, J. Birkbeck, D. J. Perello, D. Dutta, M. Ben-Shalom, T. Taniguchi, K. Watanabe, T. Holder, R. Queiroz, A. Principi, A. Stern, T. Scaffidi, A. K. Geim, and S. Ilani, Nature (London) **576**, 75 (2019).

[14] S. Samaddar, J. Strasdas, K. Janßen, S. Just, T. Johnsen, Z. Wang, B. Uzlu, S. Li, D. Neumaier, M. Liebmann, and M. Morgenstern, Nano Lett. **21**, 9365 (2021).

[15] E. Mönch, S. O. Potashin, K. Lindner, I. Yahniuk, L. E. Golub, V. Y. Kachorovskii, V. V. Bel'kov, R. Huber, K. Watanabe, T. Taniguchi, J. Eroms, D. Weiss, and S. D. Ganichev, Phys. Rev. B **105**, 045404 (2022).

[16] Z. J. Krebs, W. A. Behn, S. Li, K. J. Smith, K. Watanabe, T. Taniguchi, A. Levchenko, and V. W. Brar, Science **379**, 671 (2023).

[17] A. Tomadin, G. Vignale, and M. Polini, Phys. Rev. Lett. **113**, 235901 (2014).

[18] C. Q. Cook and A. Lucas, Phys. Rev. Lett. **127**, 176603 (2021).

[19] X. Huang and A. Lucas, Phys. Rev. B **103**, 155128 (2021).

[20] A. Levchenko and J. Schmalian, Ann. Phys. **419**, 168218 (2020).

[21] S. Li and A. Levchenko, Phys. Rev. B **105**, L241405 (2022).

[22] I. Torre, A. Tomadin, A. K. Geim, and M. Polini, Phys. Rev. B **92**, 165433 (2015).

[23] L. Levitov and G. Falkovich, Nat. Phys. **12**, 672 (2016).

[24] V. Ryzhii, M. Ryzhii, A. Satou, V. Mitin, M. Shur, and T. Otsuji, in *2022 47th International Conference on Infrared, Millimeter and Terahertz Waves (IRMMW-THz)* (IEEE, 2022).

[25] M. Ryzhii, V. Ryzhii, T. Otsuji, V. Mitin, and M. S. Shur, Appl. Phys. Lett. **120**, 111102 (2022).

[26] A. Satou, Y. Koseki, T. Watanabe, V. V. Popov, V. Ryzhii, and T. Otsuji, in *SPIE Proceedings*, edited by M. F. Anwar, T. W. Crowe, and T. Manzur (SPIE, 2016).

[27] Y. Koseki, V. Ryzhii, T. Otsuji, V. V. Popov, and A. Satou, Phys. Rev. B **93**, 245408 (2016).

[28] P. Cosme and H. Terças, ACS Photonics **7**, 1375 (2020).

[29] P. Cosme and H. Terças, Appl. Phys. Lett. **118**, 131109 (2021).

[30] G. R. Aizin, J. Mikalopas, and M. Shur, Phys. Rev. B **93**, 195315 (2016).

[31] I. O. Zolotovskii, Y. S. Dadoenkova, S. G. Moiseev, A. S. Kadochkin, V. V. Svetukhin, and A. A. Fotiadi, Phys. Rev. A **97**, 053828 (2018).

[32] Y. Dong, L. Xiong, I. Y. Phinney, Z. Sun, R. Jing, A. S. McLeod, S. Zhang, S. Liu, F. L. Ruta, H. Gao, Z. Dong, R. Pan, J. H. Edgar, P. Jarillo-Herrero, L. S. Levitov, A. J. Millis, M. M. Fogler, D. A. Bandurin, and D. N. Basov, Nature (London) **594**, 513 (2021).

[33] P. Cosme, J. S. Santos, J. P. Bizarro, and I. Figueiredo, Comput. Phys. Commun. **282**, 108550 (2023).

[34] K. J. A. Ooi and D. T. H. Tan, Proc. R. Soc. A. **473**, 20170433 (2017).

[35] J. D. Cox and F. J. García de Abajo, Acc. Chem. Res. **52**, 2536 (2019).

[36] J. W. Han, M. L. Chin, S. Matschy, J. Poojali, A. Seidl, S. Winnerl, H. A. Hafez, D. Turchinovich, G. Kumar, R. L. Myers-Ward, M. T. Dejarld, K. M. Daniels, H. D. Drew, T. E. Murphy, and M. Mittendorff, Adv. Photon. Res. **3**, 2100218 (2022).

[37] J. L. Figueiredo, J. P. S. Bizarro, and H. Terças, New J. Phys. **24**, 023026 (2022).

[38] A. J. Chaves, N. M. R. Peres, G. Smirnov, N. Asger Mortensen, and N. A. Mortensen, Phys. Rev. B **96**, 195438 (2017).

[39] J. E. Avron, J. Stat. Phys. **92**, 543 (1998).

[40] B. N. Narozhny and M. Schütt, Phys. Rev. B **100**, 035125 (2019).

[41] W. Chen and W. Zhu, Phys. Rev. B **106**, 014205 (2022).

[42] A. J. Friedman, C. Q. Cook, and A. Lucas, arXiv:2202.08269 (2022).

[43] G. Manfredi and F. Haas, Phys. Rev. B **64**, 075316 (2001).

[44] F. Haas, *Quantum Plasmas*, Springer Series on Atomic, Optical, and Plasma Physics (Springer New York, New York, NY, 2011), Vol. 65.

[45] M. Shur, *Physics of Semiconductor Devices* (Prentice Hall, 1990).

[46] D. Svintsov, V. Vyurkov, V. Ryzhii, and T. Otsuji, Phys. Rev. B **88**, 245444 (2013).

[47] S. Ali, W. M. Moslem, P. K. Shukla, and I. Kourakis, Phys. Lett. Section A: General, Atomic and Solid State Physics **366**, 606 (2007).

[48] F. Haas and I. Kourakis, Plasma Phys. Controlled Fusion **57**, 044006 (2015).

[49] R. Z. Sagdeev and A. A. Galeev, *Nonlinear Plasma Theory* (W. A. Benjamin, Inc., New York, NY, 1969).

[50] R. Z. Sagdeev, D. A. Usikov, and G. M. Zaslavsky, *Nonlinear Physics: From the Pendulum to Turbulence and Chaos* (Harwood Academic Publishers, 1988).

[51] T. Taniuti and C. C. Wei, J. Phys. Soc. Jpn. **24**, 941 (1968).

[52] T. Taniuti and N. Yajima, J. Math. Phys. **10**, 1369 (1969).

[53] T. Taniuti and K. Nishihara, *Nonlinear Waves* (Pitman Advanced Publishing Program, 1983).

[54] H. Leblond, J. Phys. B: At. Mol. Opt. Phys. **41**, 043001 (2008).

[55] M. Bartuccelli, P. Carbonaro, and V. Muto, Lettere Al Nuovo Cimento Series **42**, 279 (1985).

[56] N. Ghosh and B. Sahu, Commun. Theor. Phys. **71**, 237 (2019).

[57] A. P. Misra and B. Sahu, Physica A **421**, 269 (2015).

[58] A. R. Seadawy, Math. Meth. Appl. Sci. **40**, 1598 (2017).

[59] J. Canosa and J. Gazdag, J. Comput. Phys. **23**, 393 (1977).

[60] J. L. Bona and M. E. Schonbek, Proc. R. Soc. Edinburgh: Section A: Math. **101**, 207 (1985).

[61] A. Jeffrey and S. Xu, Wave Motion **11**, 559 (1989).

[62] Z. Feng, Wave Motion **38**, 109 (2003).

[63] M. Ablowitz and A. Zeppetella, Bull. Math. Biol. **41**, 835 (1979).

[64] I. Kourakis, S. Sultana, and F. Verheest, Astrophys. Space Sci. **338**, 245 (2012).

[65] V. E. Zakharov and L. A. Ostrovsky, Physica D **238**, 540 (2009).

[66] I. Kourakis, N. Lazarides, and G. P. Tsironis, Phys. Rev. E **75**, 067601 (2007).

[67] D. H. Peregrine, J. Aust. Math. Soc. Series B, Appl. Math. **25**, 16 (1983).

[68] V. E. Zakharov and A. A. Gelash, Phys. Rev. Lett. **111**, 054101 (2013).

[69] N. J. Zabusky and M. D. Kruskal, Phys. Rev. Lett. **15**, 240 (1965).